Multi-physics Modeling of 3D Bioprinting of Polycaprolactone Scaffolds for in-Space Additive Manufacturing

Kishore MN[1], Dong Qian[1], Wei Li[1]

[1]Department of Mechanical Engineering, The University of Texas at Dallas, TX, USA

ABSTRACT

Bioprinting in Space is a novel biofabrication process that utilizes the additive manufacturing technique to print scaffolds made of highly viscous polymer. These sacrificial scaffolds can provide vascularization of the bioprinted tissues. Like on earth, under microgravity, bioprinting parameters play an important role in determining the shape of printed filaments, and the build accuracy (e.g. shape, and dimension) of the constructs. However, challenges emerge with difficulties in predicting the flow behavior, heat, and mass transfer of high-resolution 3D bioprinted layers and their effect on the printed filament shapes. In this research, a computational fluid dynamics (CFD) model is developed to investigate and predict the effect of microgravity conditions on the bioprinting of the polycaprolactone (PCL) scaffolds. The CFD model identifies key differences between the on-earth and microgravity conditions. The results show that the PCL scaffold under microgravity is 41.5% bigger in cross-section compared to the on-earth conditions printed scaffold. Further, the shape of the PCL scaffold cross-section is more oval-ellipse shape on-earth whereas, this shape has transformed to a rhombus shape under microgravity. Such drastic changes in shape and size could potentially affect the scaffold's vascularization performance. Hence, the effect of heat transfer, surface tension, viscous force, inertia force, and gravity forces under microgravity conditions for the bioprinting of PCL scaffolds is comprehensively studied using the CFD model.

Keywords: Bioprinting, polycaprolactone, computational fluid dynamics, scaffolds, in-Space additive manufacturing, extrusion, fused deposition model.

1. INTRODUCTION

Bioprinting [1–4] under microgravity conditions that are found in space has many applications [5–7]. It could be used to print tissues and organs that are like those found in the human body [8,9]. The lack of gravity allows the cells to grow and differentiate in a way that is like the way they grow in the body [10,11]. In specific, the tissues and organs that are more resistant to the effects of gravity such as bones and blood vessels can be printed under microgravity conditions [12]. Bioprinting under microgravity conditions can be useful for long-term space missions, particularly in space-based research and development [13,14].

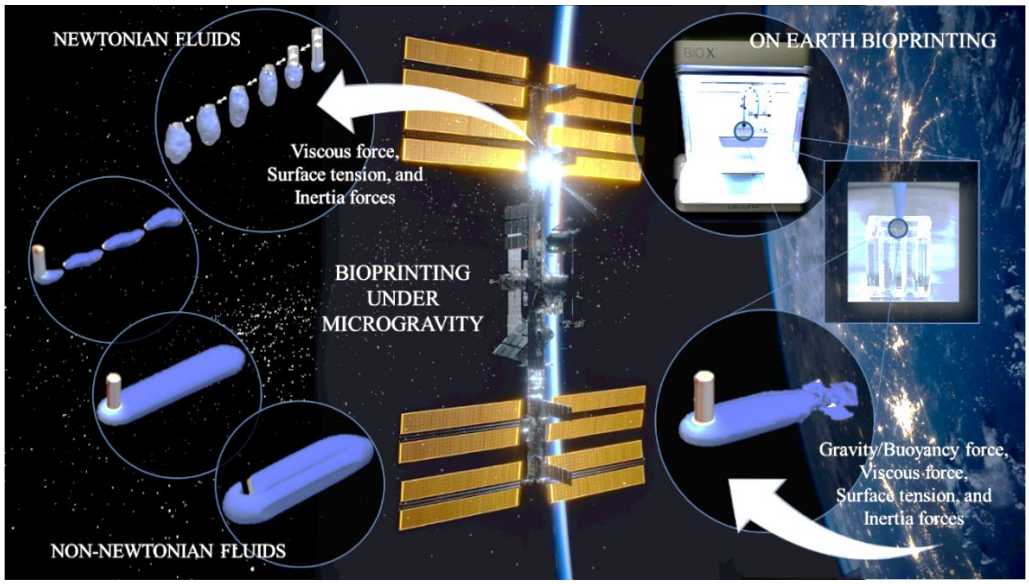

Figure 1: The illustration of bioprinting of non-Newtonian fluid flow under microgravity and on-earth conditions

In general, microgravity conditions, also known as near-zero gravity, are conditions in which objects appear to be near weightlessness. It is characterized by a reduced gravitational field which can be achieved by being in orbit around Earth as an example of the International Space Station. Microgravity can affect the behavior of fluids, and gases making it a useful environment for studying a wide range of scientific phenomena [15]. For example, a Newtonian fluid such as water exhibiting a linear relationship between the shear stress and the resulting shear rate will still behave according to its defining characteristics under microgravity conditions [17,18]. However, due to a lack of buoyancy in microgravity, Newtonian fluids will not form based on density. Thus the challenge arises in terms of predicting fluid forms as shown in Figure *1* and its control [16].

It is more challenging if the fluid is non-Newtonian since the fluid can exhibit different behaviors depending on its rheological characteristics [17,18]. However, non-Newtonian fluids can be used in a variety of applications in microgravity, including regenerative medicines, and the controlled release of drugs [19,20]. Polymers such as polycaprolactone (PCL) can be used as biomaterials which are materials that contain living cells that can be printed into specific shapes using bioprinting. However, under microgravity, since the force of gravity is greatly reduced, it is challenging to assess the effect of different forces acting during the PCL printing by conducting microgravity-specific experiments [21].

Despite these challenges, PCL-based biomaterials through bioprinting have the potential to revolutionize the field of regenerative medicines. Since long-term exposure of humans to space conditions with less or no possibility of returning for medical treatment exhibits the next logical step of having to consider medical infrastructure on board a space station [22–25]. Currently, the most widely used bioprinter for PCL-based non-Newtonian fluids is extrusion-based devices. The PCL powders melted in the nozzle and extruded using pneumatic pressure. These biomaterials in the form of scaffolds help tissue regeneration. However, the main challenge for such key experiments is the unpredictive behavior of the PCL to form the filament shape based on its printing parameters. Specifically under microgravity conditions, in the absence of gravity, the buoyancy force due to the density difference is negligible. In that case, the PCL printed flow patterns can be largely attributed to three different dominant forces. These are the viscous forces, surface tension forces, and inertia forces.

Addressing the challenge of printability under microgravity conditions required expensive real-time experiments in either an international space station [26] or creating expensive reduced gravity experimental setups on Earth. Therefore, there is a need to minimize the cost and time for trial-and-error by implementing a numerical solution capable of predicting the effect of gravity on the filament shapes under different extrusion bioprinting process parameters. Numerical models have proven to be advantageous in understanding the effect of additive manufacturing processes such as extrusion-based three-dimensional printing (3D printing – 3DP). It helps to study the flow characteristics of the fused deposition modeling process.

In this work, a computational fluid dynamics model is established to model the extrusion-based bioprinting process under regular on-earth conditions and microgravity conditions in Space. This model provides a detailed modeling route to investigate the printability of the commonly used

biomaterials (polycaprolactone (PCL)) polymers during the extrusion-based bioprinting process. Furthermore, for on-earth conditions, both experiments and computational modeling are performed to investigate the morphology of multi-layer PCL print and the underlying flow phenomena for several printing conditions. Findings from the current study will further provide reference data for a deeper understanding of the 3D bioprinting process with shear-rate-dependent viscosity and optimization of process parameters. The model can effectively evaluate the flow characteristics through the nozzle output to the multilayer and multitrack formations. With the help of the model, this research aims to investigate the effect of gravity, buoyancy force, viscous force, inertia, and surface tension forces on printed PCL scaffolds.

2. COMPUTATIONAL FLUID DYNAMICS MODELING

A computational fluid dynamics model was developed using the commercial code FLOW3D [27–30]. The computational domain is illustrated by Figure *2*, which includes the tip of the full printing nozzle head geometry along the melted PCL moving direction where a symmetric-plane boundary condition is used. The nozzle diameter is $D = 400\mu m$. The printing moves in the three mutually perpendicular directions according to the grid pattern designed. For the initial conditions, the PCL fills up the nozzle head so ϕ=1 as indicated in blue color in the nozzle, and the concentration in the air box is ϕ=0. The Grid pattern is printed with a dimension of 5mm×5mm in-plane dimension. This grid pattern has two edge lines and two middle lines movement in each in-plane direction.

When the melted PCL reaches the moving substrate, it attaches to the substrate and spreads the filament with a certain width and thickness. And then moves with it due to a high viscosity under lowered wall shear and good wettability with the substrate. It is reasonable to assume an incompressible, laminar flow condition for the process which is governed by the Navier-Stokes Eq.1 and the continuity Eq.2 [31].

$$\rho\left(\frac{\partial \mathbf{u}}{\partial t} + \mathbf{u}\cdot\nabla\mathbf{u}\right) - \nabla\cdot\left(\mu(\nabla\mathbf{u} + \nabla\mathbf{u}^T)\right) + \nabla p = \boldsymbol{F_{st}} \quad (1)$$

$$\nabla\cdot\mathbf{u} = 0 \quad (2)$$

where ρ is fluid density (kg/m^3), μ is the dynamic viscosity ($N\cdot s/m^2$) of the fluid mixture, **u,** and p represent represents the velocity (m/s) and pressure (Pa), respectively, and $\boldsymbol{F_{st}}$ is the surface tension force. The convection of the reinitialized level set function is described by:

$$\frac{\partial \phi}{\partial t} + \mathbf{u} \cdot \nabla \phi + \gamma_r[(\nabla \cdot (\phi(1-\phi)\frac{\nabla \phi}{|\nabla \phi|})) - \epsilon \nabla \cdot \nabla \phi] = 0 \qquad (3)$$

The thickness of the transition layer is controlled by the parameter ϵ, a well-educated guess which takes the value of $\epsilon = h_c/2$, where h_c is the mesh size near the nozzle tip region. γ_r represents the amount of reinitialization, which can use the maximum flow velocity magnitude. Besides defining the fluid interface, the density, and viscosity jumps across the interface are also smoothed by the level set function $\rho = \rho_{air} + (\rho_{ink} - \rho_{air})\phi$, $\mu = \mu_{air} + (\mu_{ink} - \mu_{air})\phi$.

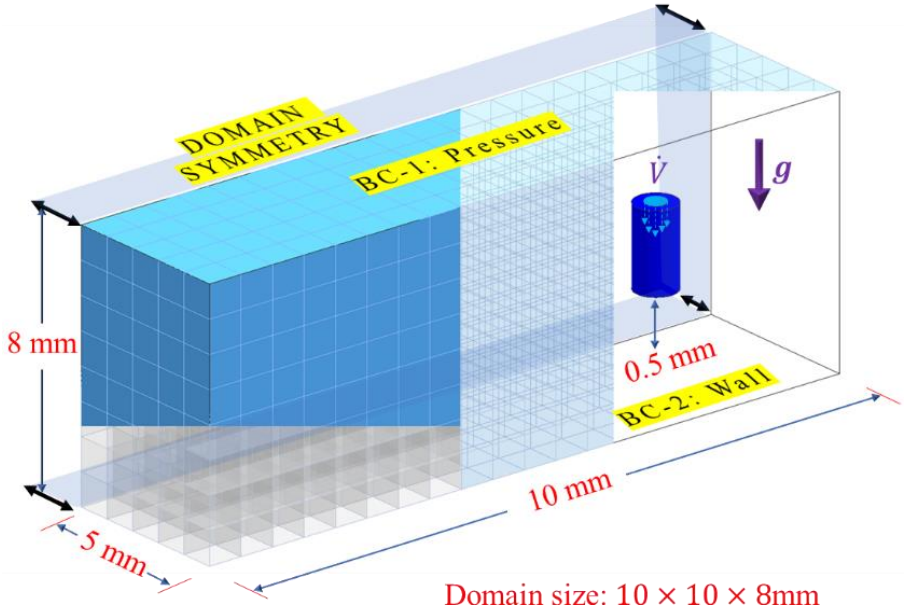

Figure 2: A computational fluid dynamics model to predict the filament shapes of the extrusion bioprinting of the PCL for on-earth and in-space printing conditions.

2.1. MODELING CONSIDERATIONS FOR MICROGRAVITY AND ON-EARTH PRINTING

Compared to on-earth modeling conditions, under microgravity, the gravity in the model was changed from 9.81m/s^2 to 0.12m/s^2. The solidus temperature was set at 60C, and the latent heat of fusion was set at 6000kJ/Kg. These two variables were increased by 10% in the microgravity conditions with a hypothesis that the solidification temperature increases with a decrease in gravity. The thermal properties were kept constant instead of temperature-dependent to study the effect of surface tension, inertia force, viscous force, and gravity forces. Further, the effect of surface tension was kept constant for both microgravity and on-earth printing conditions. The reason for this was to use the Bond number as a reference to distinguish between microgravity and on-earth printing.

Likewise, the Bo for on-earth printing was 6.3 based on the nozzle diameter of 400μm, and it is 0.07 for microgravity conditions. The change in dynamic viscosity throughout the printing was captured to study the effect of viscous forces. The fluid velocity was captured throughout the printing to study the effect of inertia forces. The mean temperature and the temperature gradient at each time step throughout printing were captured to study the effect of thermal diffusion. Under the influence of reduced gravity, the effect of gravity forces, surface tension, viscous forces, and inertia forces was studied using non-dimensional numbers and their change throughout the printing of the scaffold. A total of three layers of grid pattern scaffolds were printed for both microgravity and on-earth printing conditions.

Furthermore, the relative non-dimensional numbers were used to verify the model investigating the effect of surface tension, inertia force, viscous force, and gravity forces. These are the Bond (Bo) number (Eq.4), Froude (Fr) number (Eq.5), Weber (We) number (Eq.6), Peclet (Pe) number (Eq.7), and Marangoni (Ma) number (Eq.9).

$$Bo = \frac{\rho \boldsymbol{g} d^2}{\sigma} \tag{4}$$

$$Fr = \frac{\boldsymbol{u}}{\sqrt{\boldsymbol{g} d}} \tag{5}$$

$$We = \frac{\rho \boldsymbol{u^2} d}{\sigma} \tag{6}$$

$$Pe = \frac{\rho\ c_p\ \boldsymbol{v}_{max}\ r_s}{k} \tag{7}$$

$$Ma = -\frac{d\sigma}{dT}\frac{L_s \Delta T}{\mu \alpha} \tag{9}$$

Continuing, the melted PCL is considered a non-Newtonian fluid to be extruded through the nozzle tip to form the filament. Its viscosity versus shear strain rate relation is taken from the literature to be fitted with the power law Eq.10,

$$\mu = m(\dot{\gamma})^{n-1} \tag{10}$$

where $m = 24.53\ Pa \cdot s$ is the fluid consistency index, $\dot{\gamma}$ is the shear rate, and $n = 0.1$ is the flow behavior. The density of the PCL is assumed to be equivalent to $1124\ kg/m^3$ and the surface tension coefficient is considered from the literature as $0.07\ N/m$. The thermal conductivity of 2W/m K, specific heat of 2000 J/Kg, and thermal expansion of 5×10^{-5} were kept constant.

3. RESULTS AND DISCUSSION

3.1. 3D BIOPRINTING OF PCL SCAFFOLDS

Figure *3* shows the three layers printed for microgravity and on-earth conditions. The printing speed was 3mm/min, and the heating temperature of the PCL inside the nozzle was set at 180C. The printing was carried out in a controlled environment of 20.15C considering it as a room temperature condition. The three layers scaffold was printed in a grid pattern that has two edge lines and two middle lines in a 5×5mm in-plane square dimension. Figure *3* represents the contour of temperature distribution at the end of the 3-layer printing process.

It was observed that the microgravity conditions were able to print all three layers with near equivalent dimensions compared to on-earth conditions. The average width and height of the first layer on earth printing were ~500μm, and ~400μm with an oval shape cross section whereas it was ~350μm, and ~400μm with a rhombus shape for microgravity conditions. Similarly, for the second layer, the oval shape got expanded from ~500μm to ~600μm, and the height got reduced from ~400μm to ~300μm. However, under microgravity, the width got increased from 350μm to 400μm, and the height got reduced from 400μm to 350μm. Interestingly this dimension was maintained during the formation of the third layer. Whereas in the on-earth conditions, the second layer was compressed height by ~20%. Further, in the third layer, the width and height during on-earth conditions were 650μm and 150μm whereas, under microgravity, it was 500μm and 400μm respectively. This shows under microgravity, the layer dimensions were maintained throughout the printing much better compared to the on-earth conditions. The gravity force has influenced the on-earth conditions of second and third-layer height.

Further Figure *4*, Figure *5*, and Figure *6* show the cross-section of layers 1, 2, and 3 respectively taken in two in-plane directions of X and Y at three different locations each. From Figure *4* in layer 1, along X-axis, due to the layer shape effect, under microgravity, the dimension of the printed structure was ~10% bigger than the on-earth printing. However, across the Y-axis, the printed structure dimension was nearly equivalent to the on-earth condition. Figure *5* shows the second layer printed on top of the first layer. On Earth, the oval shape first layer cross-section has influenced the second layer cross-section to be a more elliptical shape which further compressed the first layer reducing the overall height. However, the rhombus cross-section shape of the first layer in the microgravity case converted into an oval shape influencing the second layer

to have a cross-section of oval shape with a width 20% bigger than the first layer. Due to the cross-section shape, the area fused between layer-1 and 2 was higher in the on-earth condition than in the microgravity condition.

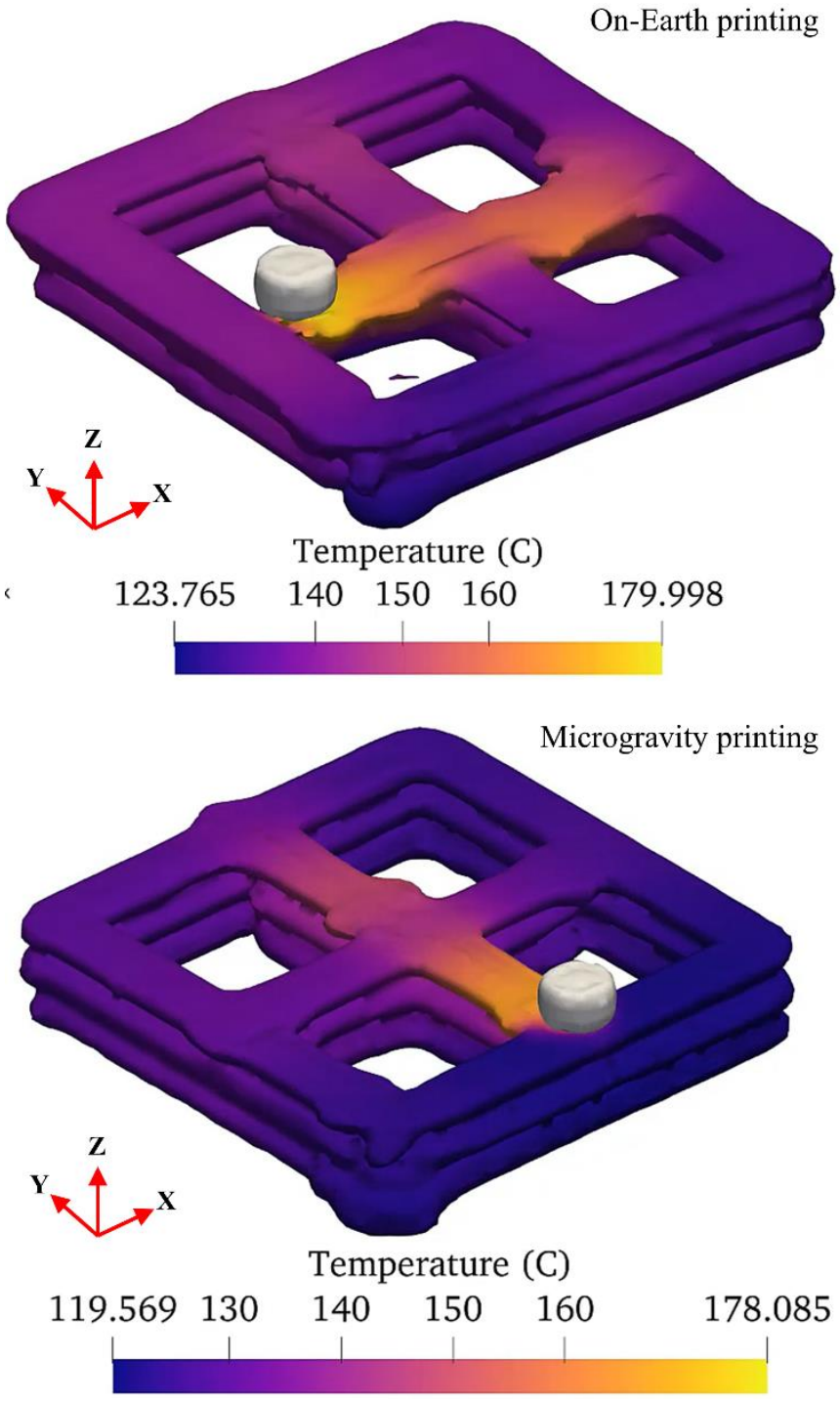

Figure 3: The three-layer bioprinting of PCL scaffold under on-earth gravity and microgravity conditions depicting the temperature distribution of the built layers.

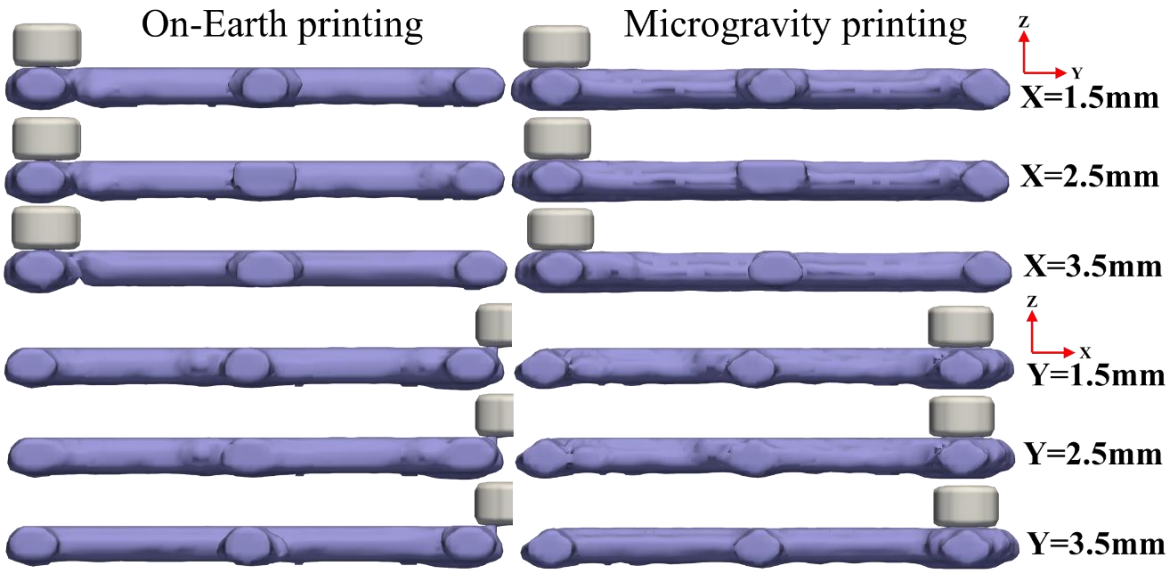

Figure 4: The first layer PCL bioprinted cross-section at X-Y plane at three different locations for on-earth and microgravity conditions.

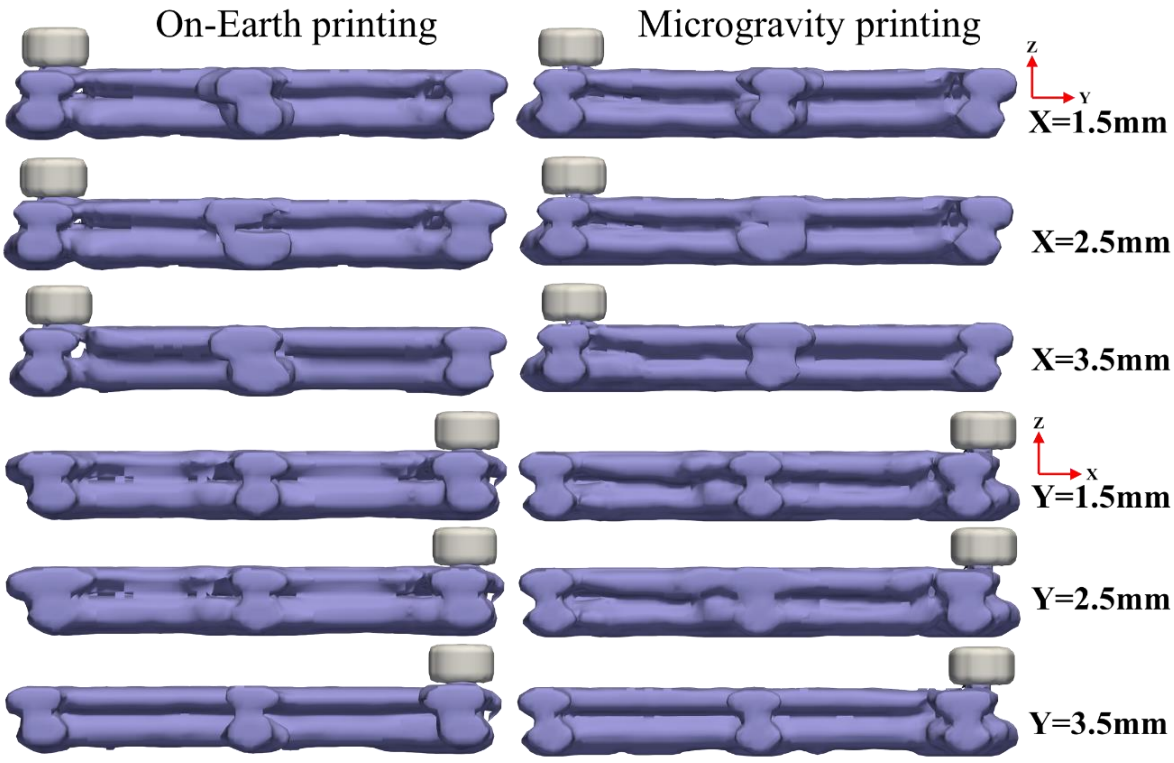

Figure 5: The second layer PCL bioprinted cross-section at X-Y plane at three different locations for on-earth and microgravity conditions.

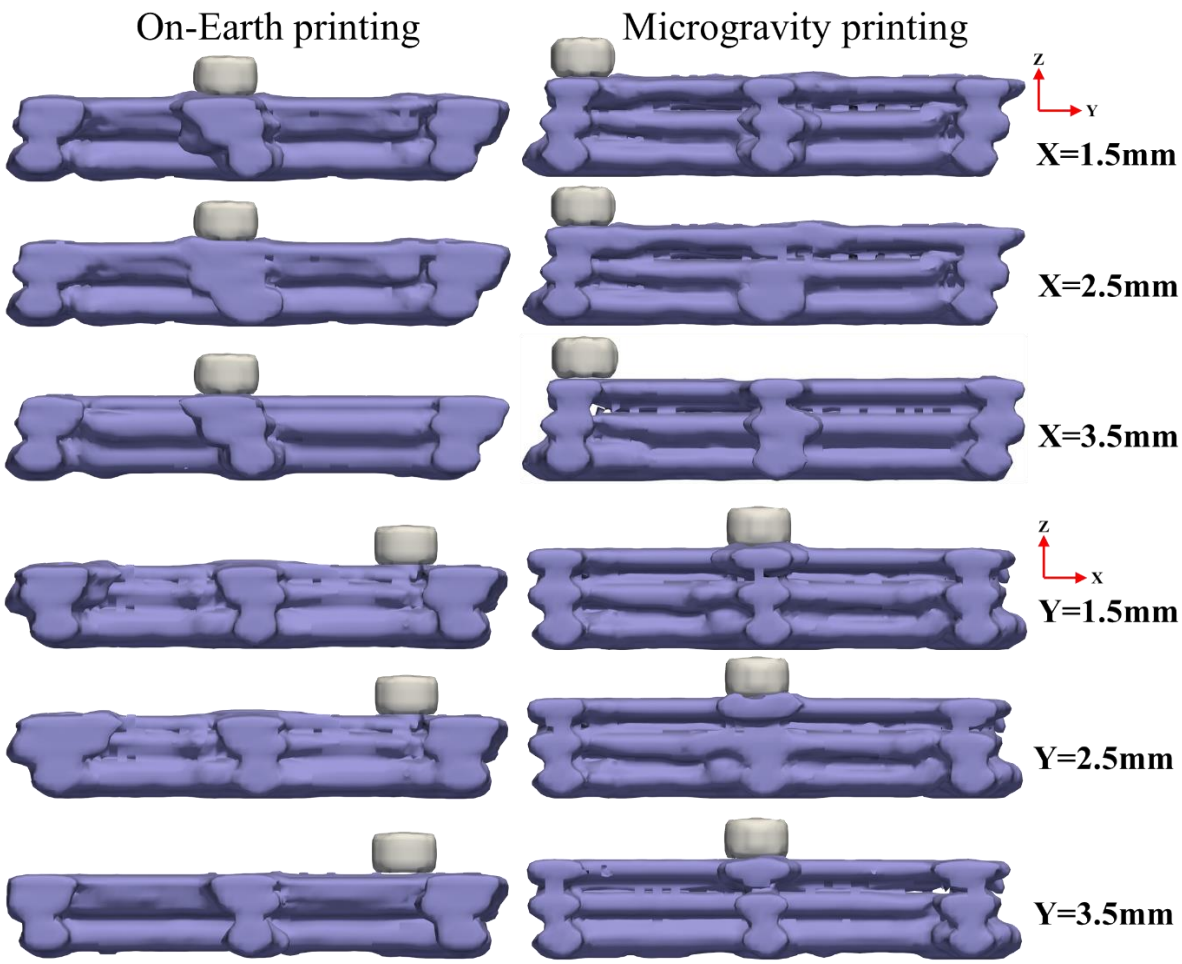

Figure 6: The third layer PCL bioprinted cross-section at X-Y plane at three different locations for on-earth and microgravity conditions.

Figure *6* represents the cross-sections of all three layers after layer-3 was printed. The influence of the cross-section shape was more predominant after printing the third layer. The oval shape of the second layer in the microgravity case helped the third layer retain its shape to an expanded oval shape. Whereas the elliptical shape of the second layer in the on-earth condition along with the gravity force has influenced the third layer to be much shorter and broader impacting the second layer. This eventually compressed the second layer and overall the height of the three layers got reduced. The influence of microgravity has reduced the swelling of the third layer and helped maintained the shape and size of the third layer. Thus microgravity can produce near-uniform layers while printing PCL compared to on-earth gravity conditions.

Figure *7* represents the temperature distribution in the entire printed scaffold for on-earth and microgravity conditions. At first, Figure *7*a represents the mean temperature extracted from the range of temperature distribution at each time step throughout the print. From the simulations,

it was observed that the temperature gradient for microgravity conditions was much steeper than for the on-earth conditions. However, up to 5 seconds, there were no differences in the temperature distribution observed. In the printing, 5 seconds cover the first layer of edge lines. The gradient was wider from the second layer start onwards. This shows that microgravity-printed layers are undergoing fast cooling compared to on-earth conditions. The temperature distribution at random time steps extracted throughout the print is shown in Figure *7*b-c. It was observed that from the second layer, the minimum temperature under microgravity was much lower than the on-earth condition. Further, the maximum temperature in most of the printed regions except near the nozzle region was lower than the on-earth condition. This shows the on-earth printed layers are still hot and semi-molten state compared to microgravity condition which is undergoing fast cooling.

From Figure *8*a, the dynamic viscosity as a measured quantity from the flow of the PCL molten fluid observed throughout the printing process was plotted against the mean temperature at each time step. It was noticed that viscous forces were dominant in the first and third layers for both on-earth and microgravity conditions. However, in the on-earth conditions, the dynamic viscosity has dropped in the second layer formation. Whenever the viscosity has dropped, the printed layer has seen a spread in the material flow with high maximum velocity. Further, in this layer, the Marangoni number was observed to be higher than the microgravity second layer (Figure *8*b). This means, in the second layer on-earth condition, temperature distribution has caused the change in surface tension to cause higher Marangoni convection. This has caused the viscosity to be reduced allowing the wider spread of the fluid flow. However, the Marangoni convection is higher in both the first and third layers under microgravity. This means both viscous force and the Marangoni convection is higher under microgravity condition. This phenomenon has helped the printed layers to maintain their shape under microgravity conditions.

Further, from Figure *8*c-d, it was observed that the Froude number is substantially higher in microgravity compared to on-earth conditions. This means, printing PCL under microgravity has experienced higher inertia forces. This has led to more mass accumulation along the printing direction. Along with higher inertia forces and viscous dominance, the resistance to change in shape and swelling movement of the fluid flow is very high in the microgravity condition. For this reason, under microgravity, the printed layers have maintained the size of the layers.

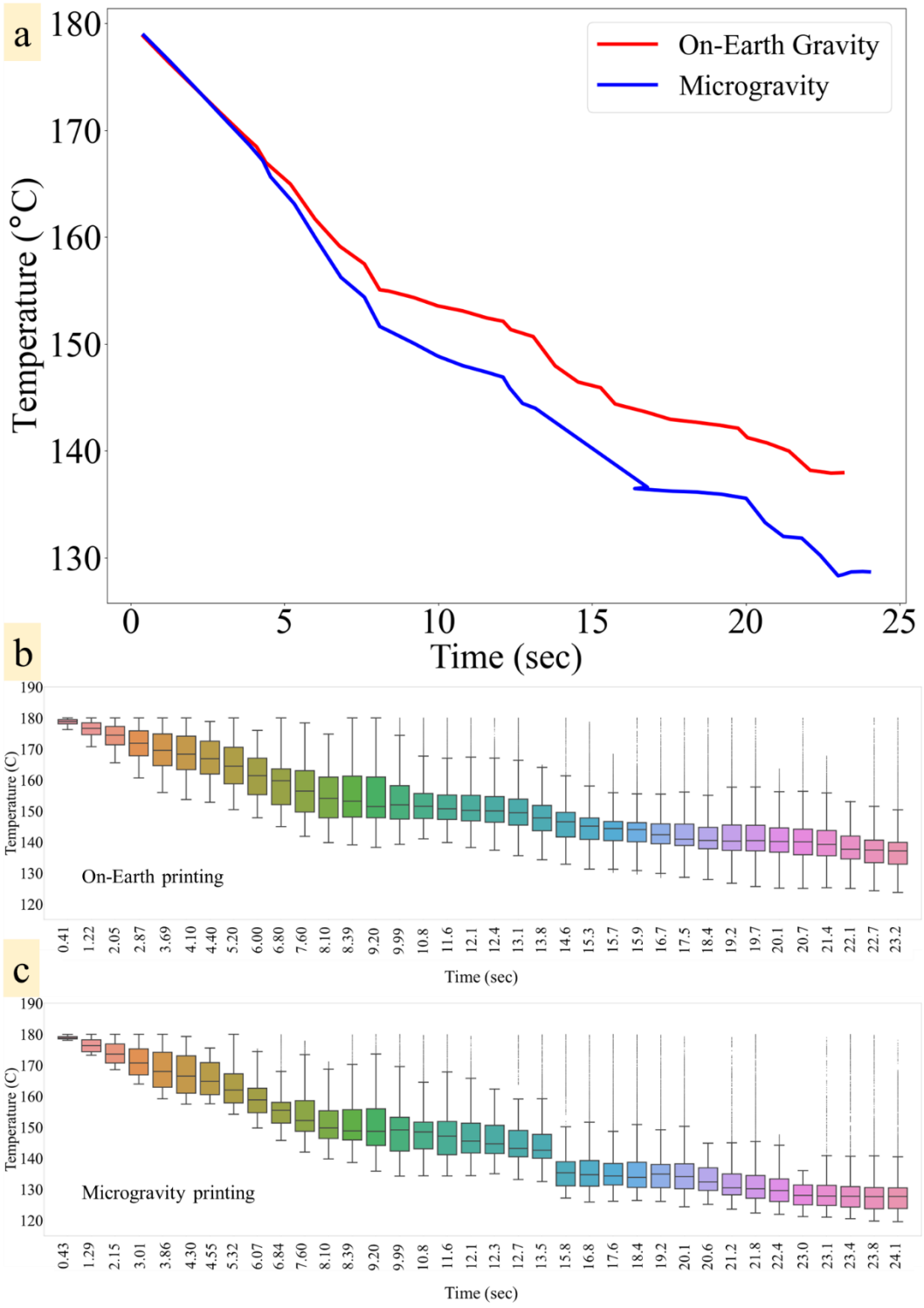

Figure 7: Temperature distribution of the three layers scaffold printed under on-earth and microgravity conditions. (a) the mean temperature extracted at each time step throughout the printing represents the temperature gradient difference between on-earth and microgravity conditions. (b) the temperature distribution extracted at random timesteps throughout the print duration for on-earth conditions and microgravity conditions (c).

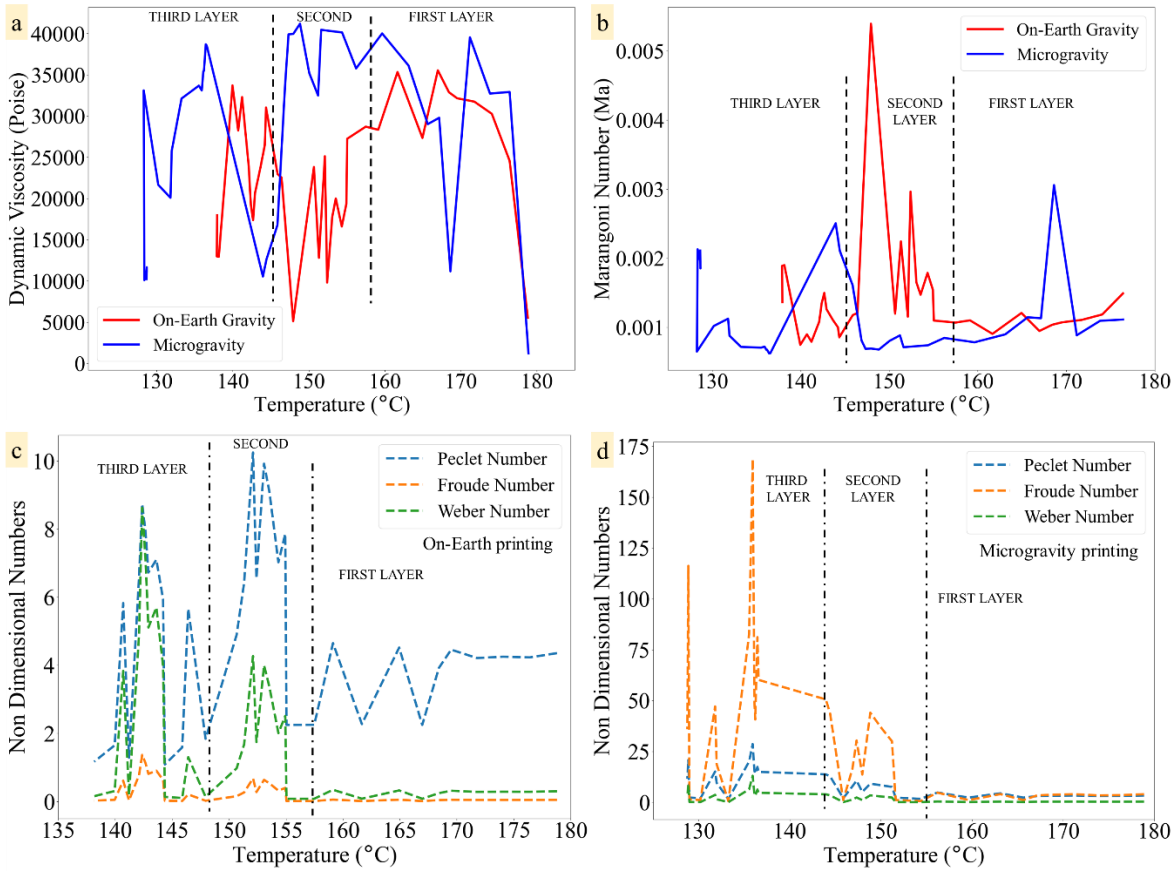

Figure 8: The three-layer printed scaffold PCL molten fluid flow characteristics during the formation of each layer representing (a) dynamic viscosity versus the mean temperature at each time step throughout the printing duration, (b) Marangoni non-dimensional number, (c-d) Peclet, Froude, and Weber non-dimensional numbers.

Furthermore, in the second and third layers, the Weber number is very low in the microgravity condition compared to on-earth (Figure *8*d). This means, the effect of surface tension as a dominant force under microgravity also participates in the maintaining of the shape of the cross-section of the printed layers. It is also to be noted that, even though, in the second and third layers under on-earth conditions, the Weber number is higher than the Froude number (Figure *8*c). This means the inertia forces are still higher in comparison with the surface tension force. Hence, under on-earth conditions, the inertia force helps maintain the size of the printed layers. It also means surface tension is not a dominant force in this condition. This is the reason behind the widespread second and third-layer cross-section elliptical shape with reduced height. Further, the Peclet number under microgravity and on-earth condition are similar in distribution. This means the heat transfer due to conduction between the layers is happening at a very slow pace. This is indeed true since the PCL has poor thermal conductivity characteristics.

4. CONCLUSION

The current research addresses the bioprinting of the PCL extrusion bioprinting process under the effect of reduced gravity or the in-space microgravity conditions through a computational fluid dynamics model. The idea behind the effort is to effectively use on-earth-based modeling considerations to predict the microgravity conditions for extrusion bioprinting of highly viscous fluids like PCL polymers. The model is versatile enough to expand it to multi-layer and multi-track simulations and effective enough to study the influence of four different forces such as gravity/buoyancy force, inertia force, viscous force, and surface tension on the printing process. The model provides in detail virtual platform to study the bioprinting process simulating on-earth and in-space microgravity conditions.

Due to high viscous fluid properties, the PCL does not behave the same as the Newtonian water fluid under microgravity conditions. The shape of the PCL cross-section on-earth conditions varies between oval and elliptical whereas it varies between Rhombus and oval under microgravity conditions. Under microgravity conditions, the shape and size of the printed layers at their desired design were better maintained compared to on-earth conditions. This uniformity of the shape and increase in size of the printed layers which is independent of the bioprinting process parameters can be utilized for regenerative medicines applications. The highly viscous fluids that are more favorable materials to be used for extrusion bioprinting in Space microgravity conditions be effectively modeled and studied using CFD modeling. The present study extends the application of computational fluid dynamics models that are yet not used to study the extrusion bioprinting process under microgravity conditions for in-space applications.

5. CREDIT AUTHORSHIP CONTRIBUTION STATEMENT

Kishore MN: Conceptualization, methodology, formal analysis, investigation, data curation, writing, visualization.

Dong Qian: Resources, supervision, project administration.

Wei Li: Resources, supervision, project administration, experimental validation.

6. DECLARATION OF COMPETING INTERESTS

The authors declare that they have no known competing financial interests or personal relationships that could have appeared to influence the work reported in this paper.

7. DATA AVAILABILITY

The limited simulation data required to reproduce these findings can be provided upon request.

8. REFERENCES

[1] D. Ke, C. Niu, X. Yang, Evolution of 3D bioprinting-from the perspectives of bioprinting companies, Bioprinting. 25 (2022). https://doi.org/10.1016/j.bprint.2022.e00193.

[2] S. V. Murphy, A. Atala, 3D bioprinting of tissues and organs, Nat Biotechnol. 32 (2014) 773–785. https://doi.org/10.1038/nbt.2958.

[3] S. Ramesh, O.L.A. Harrysson, P.K. Rao, A. Tamayol, D.R. Cormier, Y. Zhang, I. V. Rivero, Extrusion bioprinting: Recent progress, challenges, and future opportunities, Bioprinting. 21 (2021). https://doi.org/10.1016/j.bprint.2020.e00116.

[4] D.B. Kolesky, K.A. Homan, M.A. Skylar-Scott, J.A. Lewis, Three-dimensional bioprinting of thick vascularized tissues, Proc Natl Acad Sci U S A. 113 (2016) 3179–3184. https://doi.org/10.1073/pnas.1521342113.

[5] C. Impey, The biomedical implications of living off-Earth, 2021. https://arep.med.harvard.edu/gmc/protect.

[6] T. Ghidini, Regenerative medicine and 3D bioprinting for human space exploration and planet colonisation, J Thorac Dis. 10 (2018) S2363–S2375. https://doi.org/10.21037/jtd.2018.03.19.

[7] L. Moroni, K. Tabury, H. Stenuit, D. Grimm, S. Baatout, V. Mironov, What can biofabrication do for space and what can space do for biofabrication?, Trends Biotechnol. 40 (2022) 398–411. https://doi.org/10.1016/j.tibtech.2021.08.008.

[8] N. Cubo-Mateo, M. Gelinsky, Wound and Skin Healing in Space: The 3D Bioprinting Perspective, Front Bioeng Biotechnol. 9 (2021). https://doi.org/10.3389/fbioe.2021.720217.

[9] N. Cubo-Mateo, S. Podhajsky, D. Knickmann, K. Slenzka, T. Ghidini, M. Gelinsky, Can 3D bioprinting be a key for exploratory missions and human settlements on the moon and mars?, Biofabrication. 12 (2020). https://doi.org/10.1088/1758-5090/abb53a.

[10] A. Sharma, R.A. Clemens, O. Garcia, D.L. Taylor, N.L. Wagner, K.A. Shepard, A. Gupta, S. Malany, A.J. Grodzinsky, M. Kearns-Jonker, D.B. Mair, D.H. Kim, M.S. Roberts, J.F. Loring, J. Hu, L.E. Warren, S. Eenmaa, J. Bozada, E. Paljug, M. Roth, D.P. Taylor, G.

Rodrigue, P. Cantini, A.W. Smith, M.A. Giulianotti, W.R. Wagner, Biomanufacturing in low Earth orbit for regenerative medicine, Stem Cell Reports. 17 (2022) 1–13. https://doi.org/10.1016/j.stemcr.2021.12.001.

[11] W. Sun, B. Starly, A.C. Daly, J.A. Burdick, J. Groll, G. Skeldon, W. Shu, Y. Sakai, M. Shinohara, M. Nishikawa, J. Jang, D.W. Cho, M. Nie, S. Takeuchi, S. Ostrovidov, A. Khademhosseini, R.D. Kamm, V. Mironov, L. Moroni, I.T. Ozbolat, The bioprinting roadmap, Biofabrication. 12 (2020). https://doi.org/10.1088/1758-5090/ab5158.

[12] S.Y.F. Lu, A.M.R. Groh, 3D bioprinting in microgravity: An end to organ donor shortages?, STEM Fellowship Journal. 7 (2021) 25–28. https://doi.org/10.17975/sfj-2021-011.

[13] Q.A. Bean, K.G. Cooper, J.E. Edmunson, M.M. Johnston, M.J. Werkheiser, INTERNATIONAL SPACE STATION (ISS) 3D PRINTER PERFORMANCE AND MATERIAL CHARACTERIZATION METHODOLOGY, n.d.

[14] R. Crockete, D. Petersen, K. Cooper, FUSED DEPOSITION MODELING IN MICROGRAVITY, n.d.

[15] H. Gu, L. Li, Computational fluid dynamic simulation of gravity and pressure effects in laser metal deposition for potential additive manufacturing in space, Int J Heat Mass Transf. 140 (2019) 51–65. https://doi.org/10.1016/j.ijheatmasstransfer.2019.05.081.

[16] M. Gelinsky, Latest advances of bioprinting in space: an interview with Michael Gelinsky, J 3D Print Med. 4 (2020) 1–4. https://doi.org/10.2217/3dp-2020-0003.

[17] A.E. Dukler, J.A. Fabre, J.B. Mcquillen, R. Vernon, GAS-LIQUID FLOW AT MICROGRAVITY CONDITIONS: FLOW PATTERNS AND THEIR TRANSITIONS, 1988.

[18] M. Ryma, H. Genç, A. Nadernezhad, I. Paulus, D. Schneidereit, O. Friedrich, K. Andelovic, S. Lyer, C. Alexiou, I. Cicha, J. Groll, A Print-and-Fuse Strategy for Sacrificial Filaments Enables Biomimetically Structured Perfusable Microvascular Networks with Functional Endothelium Inside 3D Hydrogels, Advanced Materials. 34 (2022). https://doi.org/10.1002/adma.202200653.

[19] I. Yu, R.K. Chen, A feasibility study of an extrusion-based fabrication process for personalized drugs, J Pers Med. 10 (2020). https://doi.org/10.3390/jpm10010016.

[20] M. Di Prima, J. Coburn, D. Hwang, J. Kelly, A. Khairuzzaman, L. Ricles, Additively manufactured medical products – the FDA perspective, 3D Print Med. 2 (2016). https://doi.org/10.1186/s41205-016-0005-9.

[21] I. Egry, G. Lohofer, I. Seyhan, S. Schneider, B. Feuerbacher2, Viscosity and Surface Tension Measurements in Microgravity1, 1999.

[22] M. Braddock, Tissue Engineering and Human Regenerative Therapies in Space: Benefits for Earth and Opportunities for Long Term Extra-Terrestrial Exploration, n.d. https://www.researchgate.net/publication/333641675.

[23] F. Aliberti, E. Paolin, L. Benedetti, G. Cusella, G. Ceccarelli, 3D bioprinting and Rigenera® micrografting technology: A possible countermeasure for wound healing in spaceflight, Front Bioeng Biotechnol. 10 (2022). https://doi.org/10.3389/fbioe.2022.937709.

[24] P. Datta, A. Barui, Y. Wu, V. Ozbolat, K.K. Moncal, I.T. Ozbolat, Essential steps in bioprinting: From pre- to post-bioprinting, Biotechnol Adv. 36 (2018) 1481–1504. https://doi.org/10.1016/j.biotechadv.2018.06.003.

[25] L.J. Rothschild, Synthetic biology meets bioprinting: Enabling technologies for humans on Mars (and Earth), Biochem Soc Trans. 44 (2016) 1158–1164. https://doi.org/10.1042/BST20160067.

[26] G.A. Badikov, E.B. Mazurin, R.M. Khamukov, Commercialization of the ISS Experiments, in: AIP Conf Proc, American Institute of Physics Inc., 2021. https://doi.org/10.1063/5.0036002.

[27] Flow Science.Inc, FLOW-3D 2022 R1, (n.d.). https://www.flow3d.com/products/flow-3d/flow-3d-2022r1/ (accessed March 7, 2022).

[28] K.M. Nagaraja, W. Li, D. Qian, V. Vasudevan, Y. Pyun, H. Lu, Multiphysics modeling of in situ integration of directed energy deposition with ultrasonic nanocrystal surface modification, International Journal of Advanced Manufacturing Technology. 120 (2022) 5299–5310. https://doi.org/10.1007/s00170-022-09082-7.

[29] W. Li, M.N. Kishore, R. Zhang, N. Bian, H. Lu, Y. Li, D. Qian, X. Zhang, Comprehensive studies of SS316L/IN718 functionally gradient material fabricated with directed energy deposition: Multi-physics & multi-materials modelling and experimental validation, Addit Manuf. 61 (2023). https://doi.org/10.1016/j.addma.2022.103358.

[30] R. Mathews, K.M. Nagaraja, R. Zhang, S. Sunny, H. Yu, D. Marais, A. Venter, W. Li, H. Lu, A. Malik, Temporally continuous thermofluidic–thermomechanical modeling framework for metal additive manufacturing, Int J Mech Sci. 254 (2023). https://doi.org/10.1016/j.ijmecsci.2023.108424.

[31] L. Zhao, L. Qi, J. Luo, J. Huang, X. Hou, Three-dimensional numerical analysis and experimental confirmation for investigating the ground-based lateral droplet ejection toward microgravity simulation, Physics of Fluids. 34 (2022). https://doi.org/10.1063/5.0100466.